EFFECT OF ANNEALING PARAMETERS ON THE SHAPE MEMORY PROPERTIES OF NITI THIN FILMS

Paper P126

Gen Satoh, Andrew Birnbaum, Y. Lawrence Yao

Mechanical Engineering, Columbia University, New York, NY, 10027, USA

Abstract

Sputter deposition was used to deposit amorphous, 1μm thick, Ti-rich NiTi films on silicon substrates which were annealed at various times and temperatures to alter their microstructure. The effects of heat treatments on the shape memory and mechanical properties of the films were analysed through temperature dependent x-ray diffraction and nanoindentation. These heat treatments were shown to affect the transformation temperatures, recovery ratios and hardness of the films and can be used as groundwork for designing laser processes for the fabrication of functionally graded shape memory devices.

Introduction

Originally observed in bulk specimens, the shape memory effect (SME) and superelasticity (SE) are characteristics shared by the class of materials called shape memory alloys (SMA). These materials generated a great deal of interest in their infancy due to their ability to recover large deformations upon heating and endure significant, seemingly elastic strains. Their widespread use, however, was hampered by their slow response times due to their large thermal mass and difficulties controlling the transformation temperatures of the material. Recently, thin-film shape memory alloys have gained popularity due to their small thermal mass and thus fast response time. Thin film SMA are of particular interest for use in micro electromechanical devices (MEMS) as actuators due to their ability to produce large forces and displacements. One particular SMA, NiTi, has been the focus of extensive research for biomedical applications due to its excellent biocompatibility and good shape memory characteristics. NiTi thin films have been applied to various MEMS applications such as micro-grippers and micro-valves [1].

Furnace annealing of thin films specimens has been shown to produce specimens that exhibit shape memory properties comparable to those of bulk materials [4]. Lee et. al [5] have characterized the nucleation and growth of NiTi crystals in amorphous sputtered films through in-situ TEM observation. Furthermore, control over transformation temperature, recoverable strain, and even biocompatibility through oxidation have been demonstrated by varying annealing parameters and deposition conditions [4,6-8].

Recently there has been interest in spatially resolved crystallization of SMA films to locally induce shape memory properties. Several groups have shown the ability to crystallize NiTi films using lasers as a heat source. Wang et. al [2] have used a continuous-wave laser to selectively crystallize a sputtered NiTi thin film on a quartz substrate while Birnbaum et. al [3] have used a melt-mediated process to achieve selective crystallization using a pulsed excimer laser. The combination of spatial control of crystalline zones via laser annealing along with control of the microstructure and shape memory properties of thin film SMA would allow the creation of functionally graded devices on which different mechanisms could be activated at different temperatures or stress levels. While lasers are ideal for spatial control of shape memory properties, they produce a highly non-uniform temporal and spatial temperature distribution on the films which complicates the study of the evolution of microstructure and shape memory properties in the processed regions. In this study, the effects of heat treatment on the shape memory and mechanical properties of NiTi thin films are studied through furnace annealing which allows more precise control over the heat treatment parameters. The relationships determined through this study will aid in the design of laser processes for the fabrication of functionally graded devices.

X-ray diffraction (XRD) and transmission electron spectroscopy (TEM), among others have been the primary methods by which both bulk and thin film SMA have been characterized. These methods have been used to determine the crystal structure, phase transformation temperatures, and precipitation behaviour of annealed specimens. The increased interest in thin film SMA also requires the use of

different characterization methods that can accurately test materials in this form. Recent studies of the micro and nano-scale properties of SMA such as NiTi have made use of nanoindentation for this purpose. Gall et. al [9] have studied the nanoindentation response of bulk, Ni-rich, superelastic, single crystal NiTi in different orientations. Nanoindentation of thin films has also been used to determine the mechanical properties of sputtered and annealed films as a function of composition and film thickness [10,11]. Nanoindentation is particularly appealing for thin film specimens since they are not easily characterized by conventional means. There remains to be, however, a systematic study on the effects of heat treatment, specifically temperature and dwell time, on the nanoindentation response of thin film Ti-rich NiTi.

In this study, the effects of ageing heat treatments on amorphous, sputtered, Ti-rich NiTi films are examined to provide insight into the evolution of microstuctures and shape memory properties in laser annealed thin films. Specifically, the effects of annealing temperature and dwell time on the transformation temperatures and mechanical and shape memory properties are characterized through the use of x-ray diffraction and nanoindentation measurements.

Background

Shape Memory and Superelasticity

The shape memory effect (SME) and superelasticity (SE) exhibited by shape memory alloys are both manifestations of a reversible crystallographic shift called the martensitic transformation. For NiTi, the high-temperature or parent phase, austenite, has a cubic (β_2) structure and is ordered like CsCl. The low-temperature phase, martensite, has a monoclinic structure which is achieved through a shear-like deformation of the parent lattice. Thermodynamically, the driving force for the transformation is the change is free energy between the austenite and martensite structures which can be written as

$$\Delta G = \pi r^2 t \Delta g_c + 2\pi r^2 \sigma + \pi r t^2 (A + B) \qquad (1)$$

where r and t are the radius and thickness of a nucleated martensitic crystal in an austenitic lattice, Δg_c is the change in chemical free energy per unit volume between the austenite and martensite, σ is the interface energy per unit area, and A and B represent the elastic and plastic strain energies associated with the martensitic crystal [12]. The transformation from austenite to martensite is favored when ΔG is negative; thus, for the transformation to occur, the change in chemical free energy must overcome the interface and elastic and plastic strain energies.

In addition to the strain energies associated with the nucleation of a martensite crystal, the introduction of precipitates through ageing can also affect the thermodynamics of the phase transformation. Ni-rich NiTi has been shown to produce Ni_4Ti_3 precipitates through ageing while Ti-rich NiTi develops $NiTi_2$ precipitates. Due to the limited solubility of Ti in NiTi, in bulk materials, $NiTi_2$ precipitates only form at grain boundaries which limits their effectiveness in changing the thermodynamic equilibrium. Sputter deposition of Ti-rich NiTi thin films, however, is able to create an unstable structure with a homogeneous distribution of excess Ti. The subsequent annealing of these films causes precipitates to form within the NiTi grains which initially form as thin-plates or GP-zones at low annealing temperatures and times [13]. These plate precipitates are coherent with the austenite matrix and their coherency strains stabilize the austenite phase resulting in a decrease in phase transformation temperatures. Increases in the annealing temperature or time cause the precipitates to become spherical in shape and lose their coherency with the austenite matrix resulting in a rise in transformation temperatures.

Nanoindentation

The indentation modulus and hardness of materials tested through nanoindentation are typically determined from the slope of the unloading curve at max load. The indentation modulus is expressed as

$$E^* = \frac{1}{2}\frac{\sqrt{\pi}}{\sqrt{A}}\frac{dP}{dh} \qquad (2)$$

where E^* represents the combined modulus of the indenter tip and the specimen, A is the contact area of the indenter, and dP/dh is the slope of the unloading curve at max load. The indentation hardness, H, for a Berkovich indenter is defined by

$$H = \frac{P}{24.5 h_p^2} \qquad (3)$$

where P is the max indenter load and h_p is the "plastic" depth from indentation [14].

For basic indentation tests the maximum load or displacement is specified and after reaching this point the indenter tip is retracted. Using equations (2) and (3), the modulus and hardness can be calculated at this displacement. By applying a small oscillating load

over the basic load curve, local unloading can be achieved at each increment in indentation depth. Using the slope of the unloading curve at each increment, material properties can be measured as a function of depth into the surface. This type of test is called a continuous stiffness measurement (CSM).

Depending on the initial structure of the film, the deformation induced by the indenter can be accommodated by different mechanisms. Films that are martensite at room temperature accommodate the indent through elastic deformation of the martensite, detwinning, and plastic deformation of the martensite. The residual imprint left in the sample after the tip is retracted is the deformation accommodated by detwinning and plasticity. Films that are austenitic at room temperature accommodate the deformation initially by elastic deformation of the austenite, the stress induced phase transformation to martensite, followed by detwinning and elastic and plastic deformation of the martensite. Plastic deformation of the austenite can also be induced depending on the level of stress required to cause the austenite to martensite phase transformation. For these films, the residual imprint is the deformation accommodated by plasticity of the austenite or martensite and any residual stress-induced martensite. Upon heating, martensitic films will transform to austenite, recovering the deformation accommodated through detwinning. The recovery ratio, defined as

$$\Phi = \frac{D_{\max} - D_r}{D_{\max}} \qquad (4)$$

where $D_{\max}$ is the residual indentation depth after unloading, and D_r is the residual indent depth after heating, and represents the level of pseudo-plastic deformation accommodated by detwinning and phase transformations.

Experimental Procedure

Ti-rich Ti-Ni thin films were deposited on silicon substrates with a 1µm ultra-low residual stress Si_3N_4 LPCVD barrier layer to prevent any interaction between the film and substrate. The films were deposited at room-temperature in a magnetron sputtering system from an equiatomic NiTi target and a pure Ti target to achieve an amorphous structure which was verified using x-ray diffraction (XRD). The composition of the film was determined by energy-dispersive x-ray spectroscopy (EDX) to be 51.8 at% Ti-Ni and the film thickness was 1µm. Ti-rich films are of particular interest when creating shape memory devices since they generally have higher transformation temperatures than Ni-rich ones. Annealing of the films was performed in a vacuum tube furnace with PID temperature control. The specimens were placed in the furnace at room temperature and the system was purged with ultra-high purity argon and evacuated prior to heating. To minimize oxidation during annealing a quartz plate was clamped to the face of the NiTi film and a pure Ti block was placed in the furnace. The Ti block was used since it preferentially oxidizes compared to the NiTi film. The Ti block was polished abrasively before each annealing test to remove any oxide growth from previous annealing steps. A schematic diagram of the annealing setup is shown in Figure 1.

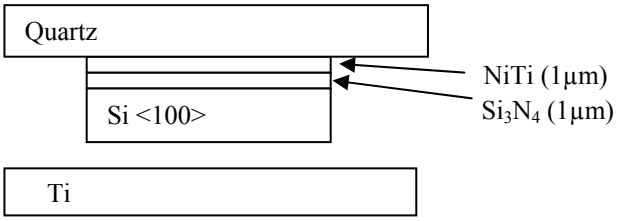

Figure 1: 1µm, 51.8 at% Ti-Ni sputter deposited film on 1µm Si3N4 barrier layer on Si substrate. Quartz placed on face to minimize oxidation during annealing. Ti plate placed in furnace as getter material.

Classical heat treatments of alloys consist of a solution treatment followed by an aging step. The solution treatment is used to homogenize the material which is then quenched to preserve its structure. The subsequent aging step is used to control the microstructure of the material. This is achieved by heating the material to a moderate temperature at which the solid solution is no longer stable, resulting in the nucleation and growth of precipitates. Since the sputter deposited Ti-rich films have an unstable, homogeneous composition similar to a quenched solid solution, no solution treatment step was performed prior to ageing. This method is also more consistent with laser annealing processes. Aging treatments were performed at four different temperatures: 460, 560, 660, and 760°C and were held at those temperatures for 5 minutes. Two additional experiments were performed for the 460°C aging treatment with dwell times of 60 and 120 minutes. After aging the samples were quenched in water to stop the precipitation process.

Following the aging treatment the films were characterized using XRD with an in-situ heating apparatus. As the temperature in the XRD was cycled the growth and decay of the austenitic peaks was recorded. The temperature at which the austenitic peaks start to emerge is the austenitic start temperature, A_s, and the temperature at which they stop growing is the austenitic finish temperature, A_f.

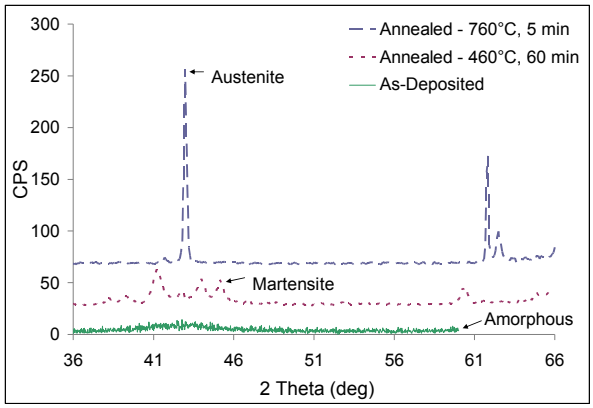

Figure 2: Room temperature XRD spectra of annealed films showing amorphous, martensite and austenite for different annealing conditions. Spectra shifted for clarity.

The martensitic start, M_s, and finish, M_f, temperatures are the temperatures at which the austenitic peaks begin to decay and disappear, respectively.

Nanoindentation was used as a means to determine the shape memory and mechanical properties of the annealed thin films. A diamond berkovich tip, a 3-sided pyramid shape, was used to produce the indents. Arrays of both the CSM and basic tests were performed on the annealed specimens. CSM measurements were performed to a depth of 1μm to characterize the full thickness of the film. Basic tests were performed to a depth of 100nm to minimize substrate effects on the material response. The residual indents were subsequently imaged using AFM to determine their initial depth. Upon heating the reverse transformation from martensite to austenite occurs, recovering some of the deformation. The indentation depths were measured again after heating to determine the recovered depth.

Results and Discussion

Figure 2 shows XRD spectra of sputtered NiTi films before and after furnace annealing. Scans were performed at room temperature to determine whether the films would exhibit shape memory, superelasticity, or if they were amorphous. The as-deposited film shows a typical amorphous spectrum with no identifiable peaks. After annealing for 5 minutes at 460°C, the film is martensitic at room temperature and will exhibit shape memory. Annealing for the same time at 760°C results in an austenitic film at room temperature which will exhibit superelasticity. XRD scans during heating (a) and cooling (b) of the <110> austenite peak for a film annealed at 560°C for 5 minutes is shown in Figure 3. These curves are typical of films that contain martensite at room temperature

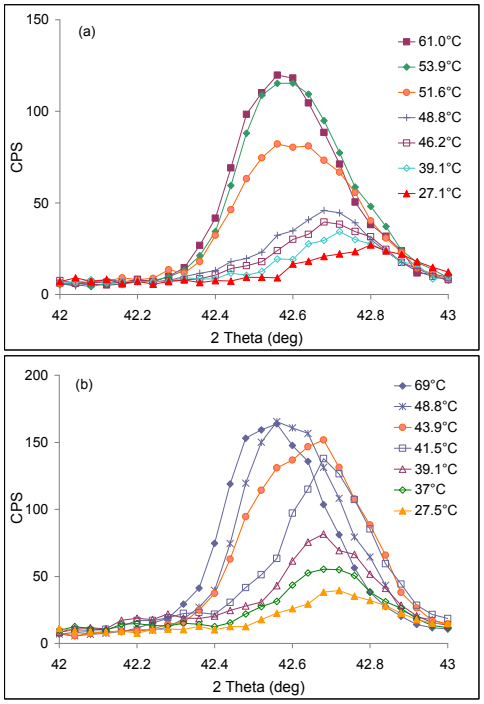

Figure 3: In-situ temperature dependant XRD spectra (typical) for film annealed at 560°C for 5 min at various temperatures showing the growth of the <110> austenite peak upon heating (a) and reduction upon cooling (b). Note existence of residual austenite at room temperature.

and are direct evidence of the reversible martensitic transformation. The initially austenitic film, however, shows no change in crystal structure upon heating. Austenite is stable at elevated temperature so no phase change is expected. The amorphous film also shows no change upon heating. Table 1 illustrates the transformation temperatures of the films annealed at different temperatures and times as determined through temperature dependent XRD measurements.

Figure 4 is an optical micrograph of indentations made in a martensitic film which was annealed at 460°C for

Table 1: Transformation temperatures for various annealing conditions. "<RT" indicates that the transformation temperature is below room temperature.

Annealing Time (min)	Annealing Temp (°C)	A_s (°C)	A_f (°C)	M_s (°C)	M_f (°C)
5	460	<RT	53.2	43.9	<RT
60	460	50.4	53	45.9	33
120	460	39.2	52.6	48	37.5
5	560	<RT	53.9	43.9	<RT
5	660	<RT	49.3	33	<RT
5	760	<RT	<RT	<RT	<RT

5 minutes. The larger 3x3 array is a set of 1µm deep CSM indentations, while the smaller array (inset) consists of nine, 100nm deep basic indents. The reference indentations are used to aid in locating the arrays under AFM. The CSM indentations are spaced 25µm apart and the basic indentations 300nm apart to minimize the effect of adjacent tests on the mechanical response. Surface relief typical of martensite is also visible over the entire film surface. Upon heating of the specimen, recovery of the 100nm indentations was observed optically, however, recovery of the CSM indentations was not apparent due to the level of plasticity involved. Figure 5 shows representative load-displacement curves for 100nm basic indentations into martensitic and austenitic films. The austenitic film shows greater recovery during unloading due to the additional deformation accommodated by the martensitic phase transformation.

It is important to note here that, in this study, the effects of annealing time and temperature are assumed to be independent. While this assumption is not strictly true, two separate temperature regimes can be identified. The thin-plate precipitates which form in Ti-rich thin films have been shown to only form for annealing temperatures below 547°C [13]. The minimum temperature was chosen to be just above the crystallization temperature of amorphous NiTi films and below the critical temperature to produce spherical precipitates. The annealing time range was chosen to allow for sufficient growth of the precipitates from plate to spherical form at the lowest annealing temperature.

Effect of Annealing Time

Phase Transformation Temperature

To determine the effect of annealing time on the shape memory properties, films were annealed for three different times at the same temperature, 460°C. Figure 6 shows the upward trend of the M_s temperature as annealing time increases. This trend is due to the coherency strains associated with $NiTi_2$ precipitate formation within the NiTi grains. The initial precipitates are coherent with the austenite matrix and stabilize the austenitic phase. Increasing the annealing time causes the precipitates to grow in size and to lose their coherency, resulting in an increase in transformation temperatures [15]. This upward trend is consistent with the work of Ishida et. al [16] who studied the phase transformation temperatures of Ti-rich films under an applied stress. Their results, however, span a much larger annealing time range and show a non-linear relationship between annealing time and transformation temperature.

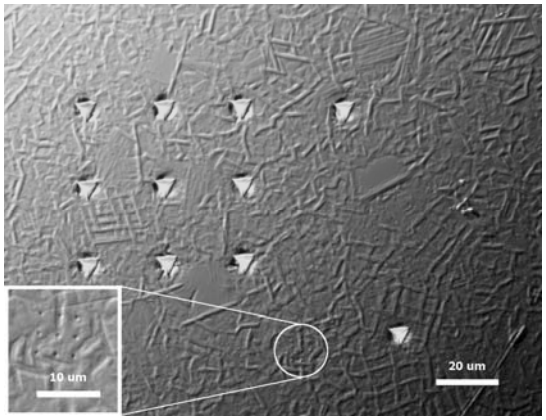

Figure 4: Optical micrograph of residual indents from 1µm and 100nm (inset) deep indents on annealed NiTi film before heating. Surface relief of martensite is visible. Film annealed at 460°C for 5 minutes.

A smaller time range was chosen for the current study since laser annealing processes typically crystallize the film over a much shorter time period. The current results show a nearly linear relationship between annealing time and martensitic start temperature.

A slight downward slope of the A_f temperatures with increased annealing time is also observed in Figure 6. This trend, combined with the increase in M_s with increasing annealing time suggests a decrease in the transformation's thermal hysteresis with increased annealing time. The thermal hysteresis of NiTi alloys is a result of a variety of mechanisms such as elastic energy dissipation and external stresses. Gabry et. al [17] have shown that the thermal hysteresis is a positive function of stress for Ti-rich NiTi specimens. Increased annealing time would allow for greater relaxation of residual stresses induced during deposition and thus reduce the hysteresis observed.

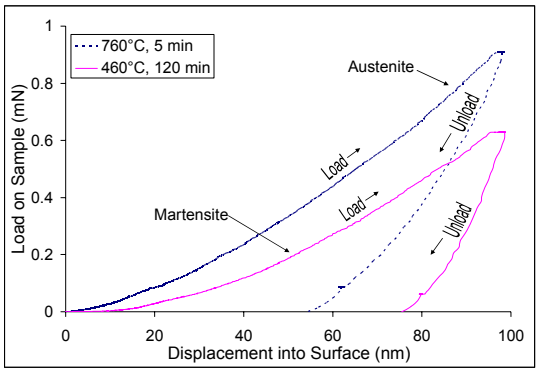

Figure 5: Representative load-displacement curves for 100nm indents in annealed films. Note smaller residual indentation depth of austenitic film due to superelasticity.

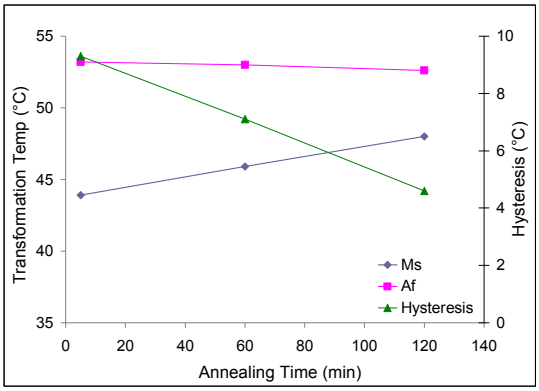

Figure 6: Phase transformation temperatures and thermal hysteresis as a function of annealing time at 460°C.

Hamilton et. al [18] have further characterized the thermal hysteresis of single crystal NiTi alloys considering the dissipation of elastic strain energy due to frictional work during the forward transformation. Elastic strain energies, "A" in equation (1), promote the reverse transformation from martensite to austenite and thus their dissipation increases the required chemical energy difference, Δg_c in equation (1), between the two phases for the transformation to occur. This has the effect of increasing the hysteresis of the phase transformation. Initially coherent precipitates in the matrix have been shown to increase the elastic energy dissipation during the transformation and thus cause increases in the thermal hysteresis. Since the coherency of the precipitates is expected to decrease with increasing annealing time, a decrease in hysteresis is expected as well.

Mechanical Response

Figure 7 is an AFM scan showing the indentation depth before and after heating of a typical martensitic film. The average depth before and after heating was determined from the array of nine, 100nm deep indents performed on each specimen. Figure 8 shows the recovery ratio of the films as defined by equation (4). The shape of the curve suggests that annealing time has little effect on the recovery ratio. For two of three annealing times the Mf temperature was found to be above room temperature and thus the films are fully martensitic at room temperature. For the third annealing time, only a slight amount of residual austenite was observed in room temperature XRD spectra. This suggests that the Mf temperature is only slightly below room temperature and that the majority of the film is martensite. Since all of the films annealed at 460°C are fully or primarily martensitic at room temperature, phase transformation strain is not

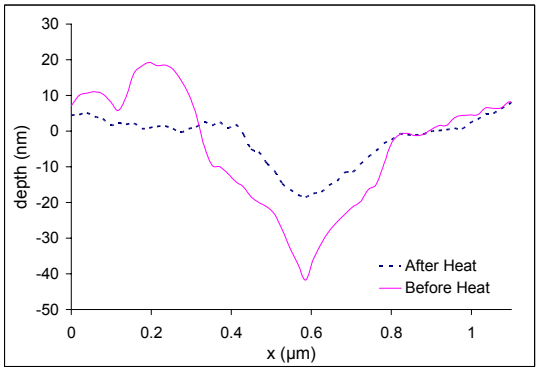

Figure 7: Typical AFM scans of indents in martensitic film before and after heating showing depth recovery. Film annealed at 460°C for 5 minutes.

expected to be a significant deformation mechanism in these specimens. Additionally, plastic deformation of the martensite is the only permanent deformation mechanism for these films. Assuming a fixed yield stress for the martensite, the recovery ratio becomes a function of the critical stress required to induce detwinning. The effect of changes in transformation temperature on this critical stress is illustrated in Figure 9, a phase diagram for NiTi in the stress-temperature domain. A change in transformation temperature between materials is represented by a shift in the transformation curves to the left or the right. For materials that are fully martensitic at room temperature, the critical stress for detwinning is nearly constant. Thus, as observed, the recovery ratio of the films should show little dependence on annealing time. Additionally, CSM indentations performed on the films showed nearly identical modulus and hardness values as a function of depth for the different annealing times.

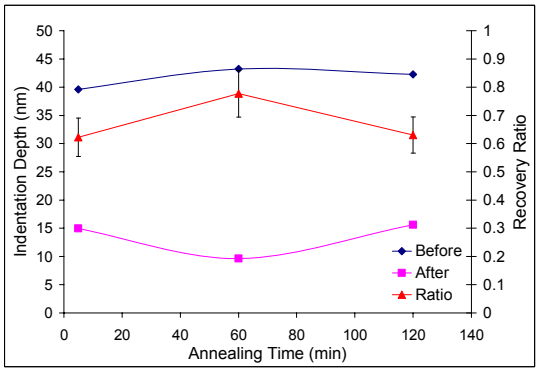

Figure 8: Indentation depth and recovery ratio as a function of annealing time for films annealed at 460°C. Error bars denote standard error.

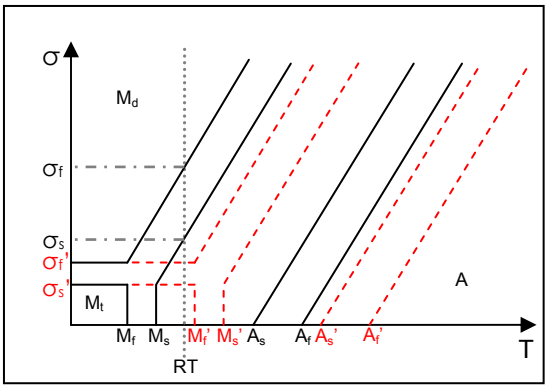

Figure 9: Schematic phase diagram for NiTi in the stress-temperature domain. Transformation temperatures and critical stresses to induce the phase transformation at room temperature, RT, are denoted Ms, M_f, A_s, A_f, σ_s, and σ_f respectively. M_d, M_t, and A denote sections where the material is fully detwinned martensite, twinned martensite, or austenite respectively. Dashed lines and primes indicate an upward shift in transformation temperatures.

This also suggests that the deformation mechanisms were the same for each of the films and occurred at similar stress levels. The level of deformation accommodated by elastic, plastic and shape memory mechanisms for each of the films is shown in Figure 10. The majority of the indentation deformation is recovered elastically upon unloading and is nearly constant with annealing time.

Effect of Annealing Temperature

Phase Transformation Temperature

The effect of annealing temperature was studied by varying the annealing temperature for a set annealing time. Figure 15 shows the change in the martensitic start temperature as a function of annealing temperature. The results show an inverse relationship between annealing temperature and phase transformation temperature. The change in transformation temperature over the range of annealing temperatures is large enough that films treated at low temperatures are martensitic at room temperature while the film treated at the highest temperature, 760°C, is fully austenitic at room temperature as can be seen in Figure 11, room temperature XRD scans which show the emergence of austenitic peaks with increasing annealing temperature. This trend is opposite to what has been observed for similar heat treatments performed by Ishida et. al on Ti-rich films [4]. As the annealing temperature is increased, diffusion becomes more active which causes the precipitates to form and grow at a higher rate. This results in larger, more spherical precipitates forming at higher annealing temperatures. These precipitates lose their coherency with the austenitic matrix and do not have the stabilizing effect of the thinner plate precipitates seen at lower temperatures. This suggests that increasing the annealing temperature should increase the phase transformation temperatures. The transformation temperatures of NiTi, both in bulk and thin film form, however, have been shown to be a strong function of composition with Ti-rich materials having higher transformation temperatures.

Changes in the composition of the NiTi matrix are the result of a few different mechanisms. As mentioned before, at equilibrium, NiTi is unable to dissolve over 0.5 at% excess Ti. The film used in this study has an unstable homogenous composition of 51.8 at% Ti – Ni as deposited and $NiTi_2$ precipitates will form during annealing. This has the effect of bringing the NiTi matrix composition closer to its equilibrium state, 50 at% Ti – Ni.

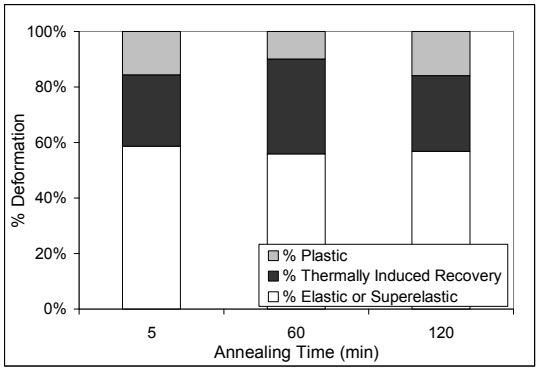

Figure 10: Percentage of indentation deformation accommodated by different mechanisms as a function of annealing time at 460°C.

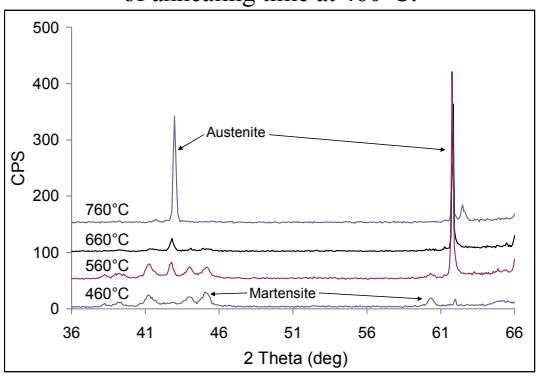

Figure 11: Room temperature XRD spectra of films annealed at different temperatures for 5 minutes. Note increase in austenitic peak intensities with increased annealing temperature.

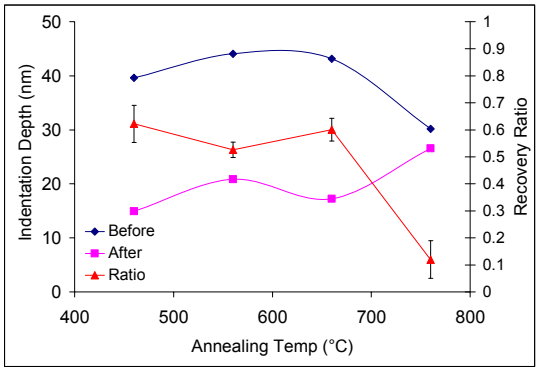

Figure 12: Indentation depth before and after heating and recovery ratio vs. annealing temperature. Error bars denote standard error

Increases in annealing temperature allows greater diffusion and thus, for the same annealing time, will cause a larger shift toward the equilibrium composition. Additional reduction in the Ti-content of the NiTi matrix is caused by the oxidation of the film. Firstov et. al [8] have shown that the oxidation rate of NiTi follows a linear trend below 500-600°C, beyond which there is exponential growth. The oxidation products are mainly Ti-oxides such as TiO_2 and TiO and are produced by consuming Ti from the NiTi matrix resulting in a further composition shift toward the Ni-rich side and a reduction in phase transformation temperatures. Despite the precautions used to minimize oxidation during annealing, oxidation of the films was observed. The discoloration of the film surface was particularly evident for higher annealing temperatures. Due to the thickness of the films, even a small layer of oxidation will cause significant changes in the matrix composition and thus transformation temperatures.

Mechanical Response

Figure 5 shows a nanoindentation load curve for a basic indent into the austenitic film which was annealed at 760°C for 5 minutes. The residual indentation depth, defined as the depth at which the load returns to zero upon unloading, is significantly lower than that of the martensitic film shown in the same figure. This is due to the added deformation accommodated by the stress-induced martensitic transformation that is recovered upon unloading. The recovery ratio as a function of annealing temperature is shown in Figure 12. For the annealing times that produce martensite at room temperature, the recovery ratio is nearly constant with temperature. However, once the room temperature structure changes to austenite, the recovery ratio upon heating decreases sharply. The slight depth recovery upon heating of the austenitic film is due to residual stress-induce martensite in the film.

The percentage of deformation accommodated by elastic, plastic, and shape memory mechanisms for the different annealing temperatures is depicted in Figure 13. The percentage of deformation accommodated by elastic deformation is nearly constant for the films annealed at 460, 560 and 660°C, but shows an increase for the films annealed at 760°C. Since the latter specimen recovers the detwinning and phase transformation strains upon unloading, these effects cannot be separated from elastic recovery, resulting in an overall increase in this value. The film annealed at 760°C also shows a larger percentage of deformation being accommodated by plasticity. As shown in Figure 9, the critical stress required to induce the phase transformation increases with decreasing transformation temperatures. If a larger stress is required to cause the transformation, a greater percentage of the film will experience stresses above the yield stress and greater plasticity will occur.

Figure 14 shows the hardness of the films annealed at different temperatures as a function of displacement into the surface. Overall, the indentation hardness

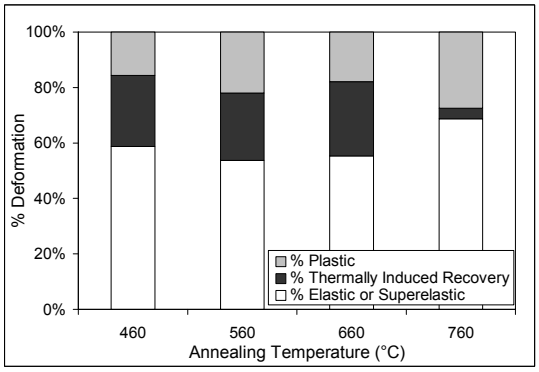

Figure 13: Percentage of indentation deformation accommodated by different mechanisms as a function of annealing temperature. Note larger superelastic recovery of austenitic (760°C) film.

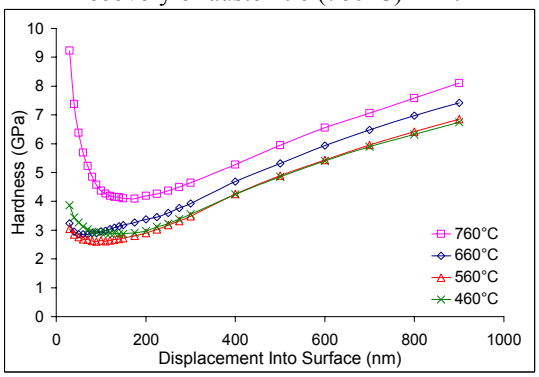

Figure 14: Hardness as a function of depth for 1µm indent films annealed at different temperatures. Note effect of substrate on hardness as depth increases.

seems to increase with increasing annealing temperature except for at shallow indentation depths. For indentation depths above 200nm, the difference in hardness between films annealed at 460 and 560°C is negligible. Increases in the annealing temperature from 560 to 760°C, however, is accompanied by an overall increase in hardness with temperature. Since all of the films are deposited on the same substrate and barrier layer, this shift is indicative of a change in the active deformation mechanisms between the films rather than substrate properties. For the fully austenitic film, as the indentation depth increases the hardness values decrease but remain higher than those of the films annealed at lower temperatures even at the maximum indentation depth of 1μm. The initial decrease in hardness is thought to be due to the relative activity of the different deformation mechanism with increasing stress. At low depths and stresses a great deal of deformation is accommodated by elastic deformation of the austenite, resulting in a high hardness values. As the indentation depth is increased phase transformation becomes a more active mechanism. Further increases in indentation depth results in a greater presence of stress-induced martensite which is accompanied by a decrease in hardness. The hardness at the maximum indentation depth does not reach that of the martensitic films since not all of the material under the indenter tip will undergo the phase transformation and the properties of the residual austenite in and around the indentation will still be felt.

The hardness of the films at a 400nm indentation depth along with martensitic start temperatures are shown in Figure 15 as a function of annealing temperature. While significant substrate effects will be seen at 400nm in a 1μm film, each film is deposited on identical substrates so the effects should be similar for each specimen. The change in hardness coincides with the change in the transformation temperature. This supports the theory that the deformation mechanism is responsible for the hardness shift. The strain accommodated by phase transformation in austenitic films is reversible upon unloading which acts as a pseudo-elastic deformation mechanism. With a greater number of reversible deformation mechanism available to austenitic films, and a larger elastic modulus than for martensite, for the same indentation depth, a greater load will be necessary and the contact area will be smaller. Both of these effects contribute to the greater hardness seen for austenitic films. The increase in hardness seen between the films annealed at 660 and 760°C is due to the volume fraction of martensite in each of the films. Annealing at 760°C produces a fully austenitic film while annealing at 660°C produces a phase mixture of martensite and austenite as determined through XRD. Using the rule of mixtures,

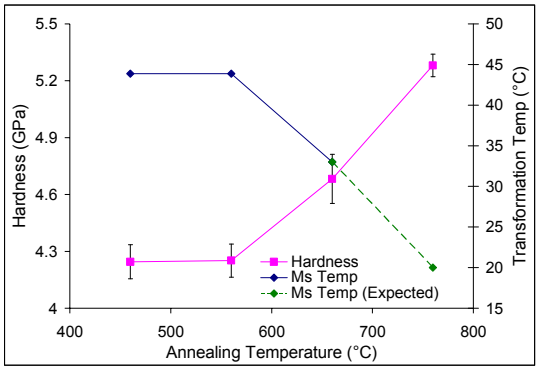

Figure 15: M_s temperature and hardness at 400nm indentation depth as a function of annealing temperature. Dashed line shows expected behavior of M_s temperature for 760°C annealing temperature which was fully austenitic at room temperature. Error bars denote standard error.

the fully austenitic films would be expected to have a higher hardness value.

Conclusion

Ti-rich NiTi films annealed at various temperatures and times have been characterized through x-ray diffraction and nanoindentation. The films exhibit a martensitic structure when annealed at low temperatures and the growth of $NiTi_2$ precipitates with annealing time results in higher transformation temperatures and a reduced thermal transformation hysteresis. Increasing the annealing temperature has been shown to decrease transformation temperatures and increase the volume fraction of austenite in the films. The recovery ratio of the films after nanoindentation was found to be dependent primarily on the room temperature phase of the film with the martensitic films showing greater thermally induced recovery due to the pseudo-plastic deformation accommodated by detwinning. Nanoindentation hardness has been shown to increase with decreasing transformation temperatures due to the addition of phase transformation strain as a pseudo-elastic deformation mechanism for austenite. These results suggest that short duration thermal treatments are an effective method of changing the shape memory and mechanical properties of Ti-rich NiTi thin films. Furthermore, these relationships can be applied to the design of laser processes for fabrication of functionally graded shape memory devices.

References

[1] Bellouard, Y. (2008) Shape memory alloys for Microsystems: A review from a material research

perspective, Materials Science and Engineering A 481-482, 582-589

[2] Wang, X., Bellouard, Y. and Vlassak, J.J. (2005) Laser annealing of amorphous NiTi shape memory alloy thin films to locally induce shape memory properties, Acta Materialia 53, 4955-4961

[3] Birnbaum, A.J., Chung, U.-J., Huang, X., Ramirez, A.G., Polvino, S. & Yao, Y.L. (2007) Melt-mediated laser crystallization of thin film NiTi shape memory alloys, in Proceedings of ICALEO – Laser Materials Processing, 98-107.

[4] Ishida, A., Takei, A. & Miyazaki, S. (1993) Shape memory thin film of Ti-Ni formed by sputtering, Thin Solid Films 228, 210-214

[5] Lee, H., Ni, H., Wu, D.T. & Ramirez, A.G. (2005) Grain size esitmations from the direct measurement of nucleation and growth, Applied Physics Letters 87, 124102-1-3

[6] Paula, A.S., Canejo, J.P.H.G., Martins, R.M.S. & Fernandes, B. (2004) Effect of thermal cycling on the transformation temperature ranges of a Ni-Ti shape memory alloy, Materials Science and Engineering A 378, 92-96

[7] Ishida, A., Sato, M. & Miyazaki, S. (1999) Mechanical properties of Ti-Ni shape memory thin films formed by sputtering, Materials Science and Engineering A 273-275, 754-757

[8] Firstov, G.S., Vitchev, R.G., Kumar, H., Blanpain, B. & Van Humbeeck, J. (2002) Surface oxidation of NiTi shape memory alloy, Biomaterials 23, 4863-4871

[9] Gall, K., Dunn, M.L., Liu, Y., Sehitoglu, H. & Chumlyakov, Y.I. (2002) Micro and macro deformation of single crystal NiTi, Transactions of the ASME 124, 238-245

[10] Tall, P.D., Ndiaye, S., Beye, A.C., Zong, Z., Soboyejo, W.O., Lee, H., Ramirez, A.G. & Rajan, K. (2007) Nanoindentation of Ni-Ti thin films, Materials and Manufacturing Processes 22, 175-179

[11] Shaw, G.A. & Crone, W.C. (2004) Direct measurement of the nanoscale mechanical properties of NiTi shape memory alloy, in Materials Research Society Symposium Proceedings: Mechanical Properties of Nanostructured Materials and Nonocomposites 791, Boston, USA, 215-220

[12] Shimizu, K. & Tadaki, T. (1987) Shape memory effect: mechanism, in H. Funakubo (ed) Shape Memory Alloys, Gordon and Breach Science Publishers, 1-60.

[13] Kajiwara, S., Kikuchi, T., Ogawa, K., Matsunaga, T. & Miyazaki, S. (1996) Strengthening of Ti-Ni shape-memory films by coherent subnanometric plate precipitates, Philosophical Magazine Letters 74, 137-144

[14] Fischer-Cripps, A.C. (2004) Nanoindentation testing, in F.F. Ling (ed) Nanoindentation, Springer, 21-38.

[15] Ishida, A., Sato, M., Kimura, T. & Sawaguchi, T. (2001) Effects of composition and annealing on shape memory behavior of Ti-rich Ti-Ni thin films formed by sputtering, Materials Transactions JIM 42, 1060-1067

[16] Ishida, A., Sato, M., Takei, A. & Miyazaki, S. (1995) Effect of heat treatment on shape memory behavior of Ti-rich Ti-Ni thin films, Materials Transactions JIM 36, 1349-1355

[17] Gabry, B., Lexcellent, C., No, V.H. & Miyazaki, S. (2000) Thermodynamic modelling of the recovery strains of sputter-deposited shape memory alloys Ti-Ni and Ti-Ni-Cu thin films, Thin Solid Films 372, 118-133

[18] Hamilton, R.F., Sehitoglu, H., Chumlyakov, Y. & Maier, H.J. (2004) Stress dependence of the hysteresis in single crystal NiTi alloys, Acta Materialia 52, 3383-3402

Meet the Authors

Gen Satoh received his B.S. from Harvey Mudd College and his M.S. from Columbia University. He is currently a doctoral student at the Manufacturing Research Laboratory at Columbia University.

Andrew J. Birnbaum received his B.S and M.S. from Carnegie Mellon University. He is currently a doctoral student at the Manufacturing Research Laboratory at Columbia University.

Dr. Y. Lawrence Yao is currently department chair of Columbia University's Mechanical Engineering Department and director of the Manufacturing Research Laboratory. He received his Ph.D. from the University of Wisconsin-Madison in 1988. He also serves on the Board of Directors of LIA.